AN EVALUATION OF THE STRESS NON-UNIFORMITY DUE TO THE HETEROGENEITY OF AC IN THE INDIRECT TENSILE TEST

Bing Zhang[1], Linbing Wang[2] and Mehmet Tumay[3]

ABSTRACT

Simple Performance Tests (SPT) including indirect tensile test and dynamic modulus test have been widely used in the evaluation of the performance of asphalt concrete. The so-called SPT tests typically apply uniform stresses on the boundary and therefore obtain the stress-strain relation with convenience. Nevertheless, asphalt concrete is a heterogeneous material composed of asphalt binder, aggregate and air void. The three constituents have drastically different stiffness. Even under a uniform boundary stress, the internal stress and strain distributions are not uniform. This paper presents a comparison between the stress distribution based on heterogeneous material properties and that based on homogeneous material properties using X-ray Computed Tomography (XCT) and Finite Element (FE) simulation. The comparison indicates that material heterogeneity is an important factor that must be considered in the characterization of asphalt concrete.

INTRODUCTION

Indirect Tensile Test (IDT) has been widely used to predict the performance in fatigue of asphalt concrete. However the interpretation of the test is based homogeneous elasticity; the microstructure or the heterogeneity of the sample is not reflected in enough details for numerical simulation historically.

Various material models have been introduced to predict the behavior of asphalt concrete under both monotonic loading and cyclic loading. Schapery (1984) introduced a model by replacing physical strains with pseudo strains so that a viscoelastic problem can be transformed into an elastic problem through the correspondence principle. Work potential theory (Schapery 1990) was used in constitutive and evolution description based on pseudo stresses and strains. The change of stiffness of the material due to accumulative damage or healing was also taken into account. Both monotonic loading

[1,2, 3] Graduate Research Assistant, Assistant Professor and Professor, Department of Civil and Environmental Engineering, Louisiana State University and Southern University, Baton Rouge, LA 70803.

and cyclic loading were investigated using this theory by Park et al (1996), Lee (1998) and Zhang et al. (1997). Viscoplastic models were also introduced recently to describe the rate dependent plastic stress - strain relations. Collop et al (2003) implemented an elasto-viscoplastic constitutive model with damage for asphalt. It was formulated based on the generalized Burger's model: an elastic element in series with a viscoelastic element (linear Voigt) and a viscoplastic element (nonlinear). A power law function was assumed for the viscoplastic strain rate-stress relationship. Damage was accounted for by introducing parameters that modify the viscosity. Tashman et al (2005) developed a microstructural viscoplastic continuum model for asphalt concrete. The viscoplastic strain rate was defined using Perzyna (1966) flow rule and the linear Drucker-Prager yield function. The aggregate anisotropy was accounted for by introducing a microstructure tensor reflecting the orientation of nonspherical particles. Seibi et al (2001) used a Perzyna type viscoplastic constitutive model with isotropic hardening and Drucker-Prager yield criteria. Schwartz et al (2002) developed a model based on the extended viscoplastic Schapery continuum damage model. Time-temperature superposition was assumed to be valid in this model. The model was compared favorably with experimental results and it was concluded that the assumption of time-temperature superposition is valid for both viscoelastic and viscoplastic strain responses.

The literatures indicate that asphalt concrete is controlled by viscoplastic response and dominated by plasticity that can be defined by Drucker-Prager criterion. However, these continuum models were based on homogeneous material properties derived from various experimental data on representative volumes or specimens. The microstructure was not considered in these models. In this study, the x-ray tomography technology was used to obtain the internal microstructure of the specimens. Image analysis method was developed to translate the acquired gray images into binary images to reconstruct the three dimensional (3D) microstructure models that reflect the geometry of voids, aggregates, and binder of the asphalt concrete specimens. This method can effectively reflect the discontinuous distribution of stresses, which is critical for damage incurrence.

This paper compares the theoretical solution for the IDT with FEM (Finite Element Method) simulations, evaluates whether a parameter, the stress concentration

factor (Wang 2003) could capture the essential performance of asphalt concrete in terms of fatigue properties.

X-RAY TOMOGRAPHY IMAGING, ANALYSIS AND MICROSTRUCTURE MODEL

X-ray Tomography is a valid tool for quantifying the microstructure of asphalt concrete (Wang et al 2001; Masad et al 2002; Wang et al 2004). The asphalt concrete sample was scanned using x-ray tomography to obtain a series of gray image slices that reflect density variation of the constituents such as asphalt binder, aggregates and voids (Figure 1). Calibration was carried out according to the material properties and the size of the samples. It is very important to obtain good images in the scanning process so that accuracy can be established from the very beginning. When multiple slices were stacked together they create 3D visualization of the internal structure of the specimen. Several computer codes, using IDL language, were written to carry out the 3D reconstructions and quantification (illustrated in Figure 2). Through image processing, the series of images were transformed into a 3D data array that can be mapped into FEM elements. Voids and aggregates were identified by setting proper thresholds in the data array. The threshold values play a critical role in this process. The proper threshold value can be obtained through comparison between image measurements and the actual void content and/or aggregate volume fractions. After identification of the material components, proper material properties (such as elastic modulus and Poison's ratio) can be assigned to the corresponding components. A FORTRAN program was written to automatically generate the simulation model to implement this methodology. Three constituents (components), asphalt binder, aggregates and voids with different material properties were considered in the simulation to account for the different mechanical properties of the constituents. With this method, only the binder is considered as a rate and temperature dependent material. Its characterization is simpler and requires much less time and efforts. A statistic study with elastic material model for small strain was conducted here to study the relative effect of mix properties on the performance of asphalt concrete and validate whether the simulation method can capture the essential data to represent performance.

THEORETICAL SOLUTION FOR INDIRECT TENSION TEST

Due to the geometry of the specimen and the loading characteristics of IDT, the stress and strain in the specimen during loading are complicated. The simplified theoretical solution for the plane stress condition along the horizontal and the vertical diameter is formulated as follows (Hondros, 1959):

Along the horizontal diameter:

$$\sigma_{11} = \frac{2P}{\pi aL}\left[\frac{\left(1-\frac{x^2}{R^2}\right)\sin 2\alpha}{1+2\frac{x^2}{R^2}\cos 2\alpha+\frac{x^4}{R^4}} - \tan^{-1}\left(\frac{1-\frac{x^2}{R^2}}{1+\frac{x^2}{R^2}}\tan\alpha\right)\right]$$

$$\sigma_{22} = -\frac{2P}{\pi aL}\left[\frac{\left(1-\frac{x^2}{R^2}\right)\sin 2\alpha}{1+2\frac{x^2}{R^2}\cos 2\alpha+\frac{x^4}{R^4}} + \tan^{-1}\left(\frac{1-\frac{x^2}{R^2}}{1+\frac{x^2}{R^2}}\tan\alpha\right)\right]$$

Along the vertical diameter:

$$\sigma_{11} = \frac{2P}{\pi aL}\left[\frac{\left(1-\frac{y^2}{R^2}\right)\sin 2\alpha}{1-2\frac{y^2}{R^2}\cos 2\alpha+\frac{y^4}{R^4}} - \tan^{-1}\left(\frac{1+\frac{y^2}{R^2}}{1-\frac{y^2}{R^2}}\tan\alpha\right)\right]$$

$$\sigma_{22} = -\frac{2P}{\pi aL}\left[\frac{\left(1-\frac{y^2}{R^2}\right)\sin 2\alpha}{1-2\frac{y^2}{R^2}\cos 2\alpha+\frac{y^4}{R^4}} + \tan^{-1}\left(\frac{1+\frac{y^2}{R^2}}{1-\frac{y^2}{R^2}}\tan\alpha\right)\right]$$

Where P is the magnitude of the applied force, a is the width of the loading plate, L and R are the length and radius of the cylinder respectively, σ_{11} and σ_{22} are the direct stresses in the horizontal and vertical directions respectively.

The 3D solution was formulated with potential function by Wijk (1978). However, it is more complicated and is close to the plane stress solution. The influence of the loading plate stiffness and geometry is in the vicinity of the plate only (Zhang, 1997). Therefore only the above equations were used to draw the stress distribution of the specimen for the purpose of comparison.

FEM MODEL CONSTRUCTION

A FEM geometry model was built to reflect the actual microstructure of the specimens (specimens are from the WesTrack project, Epps et. al, 1997). By importing the three dimensional data obtained from image analysis and reconstruction, the elements representing aggregates and voids are grouped and separated from the elements representing binder or mastics. Element groups representing aggregates and asphalt binders were assigned with different elastic or viscoplastic material properties while the element group for voids was removed during the loading steps. In this study, all the non-voids components were assigned with elastic properties that may represent the behavior of the binder at low temperature and small loading magnitude. The result of the FEM simulation was compared with the analytical elastic solution to verify the accuracy of FEM simulation so that proper mesh size can be determined. Due to the large memory and disk space requirement of the simulation, all the images with 512*512 resolution were transformed into 100*100 resolution and the volume fractions of the constituents were maintained. In addition to stresses, strains and displacements that result from the FEM simulation, the stress concentration factor (the ratio between the largest tensile stress and that of the elastic solution assuming homogeneity) was also computed. The stress concentration factor is a comprehensive indicator of the rationality of the material structure. To validate these concepts, the three mixtures of the WesTrack project (the fine mix, the fine plus mix, and the coarse mix) were evaluated using the procedure developed. The results will be discussed later.

RESULTS AND DISCUSSIONS

Due to the existence of aggregates and voids in the mixture, the stress distribution no longer follows that of either the theoretical elastic solution or the FEM solution assuming homogeneity of the material.

The typical stress distributions along vertical and horizontal diameter for these three samples are plotted in Figure 3 through Figure 5. It can be seen that the coarse mix had the largest stress variations, followed by the fine plus mix and the fine mix. It should be note that his order is the same order that these mixes performed (from poor to good).

The analytical solution for the IDT test model used in the FEM simulation was calculated and illustrated in Figure 6. While assigning the same property for aggregate and asphalt binder, the two-constituent FEM model yields a solution that agrees well with the analytical elastic solution in the average sense.

By comparing the stress distributions of the FEM simulations that include voids, aggregates and binder and those of the analytical solution, one can obtain the stress concentration factor conveniently. It is found that the fine mix sample had the least stress concentration while the coarse mix showed the largest stress concentration (See Figure 7). However, the stress concentrations are similar if voids were not removed, indicating the importance of void structure on the behavior of the mixture. In the calculation of the average stress (needed for calculating the stress concentration factor), the stresses along the 20mm and the 80 mm position (with a height of 60mm) were averaged to avoid the local effect in the vicinity of the loading plate. The results are tabulated in Table 1. This result may imply that the fine mix will have the best performance, which was observed in the field experiment.

The simulations are for thin disks. Generally, the stress distribution for all fine mix specimens (thin disks) is consistent, and so is for the coarse mix specimens and the fine plus mix specimens, indicating that thin disks may be used for simulations to reduce memory and time requirements. In order to verify the statistic consistency of the simulations, ten simulations were performed for each mixture. The average stress and its standard deviations were collected for every simulation. The results (Table 2 to Table 4) show that for every sample(a mix), the consistency is good and therefore the solutions were distinguishable among the three mixtures of the WesTrack project.

The variation of stress distribution due to the different ratios between the elastic modulus of aggregates and that of asphalt binder was also studied by comparing simulation results of samples with 1:1 ratio (aggregate modulus to binder or mastic modulus) up to 100:1 ratio. The results were plotted in Figure 8 for stresses along vertical and horizontal diameters respectively. It can be seen that large difference in constituent properties will lead to significant stress concentration even if there were no voids presented. This indicates that the relative stiffness between aggregates and the asphalt binder (or mastics) also plays an important role in the mixture performance. It also

implies that the damage may become more significant due to a softer binder or mastics. It should be noted that for the simulations with E ratio of 20:1 and 100:1, more refined mesh might be needed to catch the accurate stress distribution and hence stress concentration.

CONCLUSIONS

This paper presents an evaluation of the non-uniform stress distribution effect on IDT test. The stress concentration varies significantly with the void distribution and the relative stiffness between aggregate and binder. IDT test should be combined with FEM simulation to offer better interpretation of the test results. The stress concentration factor may serve as a good simple performance indicator.

REFERENCES

Collop, A. C., Scarpas, A., Kasbergen, C, and Bondt A. (2003). "Development and finite element implementation of a stress dependent elasto-visco-plastic constitutive model with Damage for Asphalt", *TRB 2003 Annual Meeting CD-ROM*.

Epps,J., Monismith, C.L, Alavi, S.H, Mitchell, T.M. (1997). WesTrack Full-Scale Test Track: Interim Findings. http://www.westrack.com/wt_04.htm

Hondros, G. (1959), "Evaluation of Poisson's Ratio and the Modulus of Materials of a Low Tensile Resistance by the Brazilian (Indirect Tensile) Test with Particular Reference to Concrete", *Australia Journal of Applied Science*, Vol. 10, No. 3, 243-268.

Lee, H.J. and Y.R. Kim (1998a), "A Uniaxial Viscoelastic Constitutive Model for Asphalt Concrete under Cyclic Loading", *ASCE Journal of Engineering Mechanics*, Vol. 124, No. 11, pp. 1224-1232.

Lee, H.J. and Y.R. Kim (1998b), "A Viscoelastic Continuum Damage Model of Asphalt Concrete with Healing", *ASCE Journal of Engineering Mechanics*, Vol.124, No.11, p.1-9.

Masad, E; Jandhyala, VK; Dasgupta, N; Somadevan, N; Shashidhar, N (2002). Characterization of Air Void Distribution in Asphalt Mixes Using X-Ray Computed Tomography. Journal of Materials in Civil Engineering. Vol.14, No.2, pp 122-129.

Park, S.W. Y.R. Kim, and R.A. Schapery (1996). "A Viscoelastic Continuum Damage Model and Its Application to Uniaxial Behavior of Asphalt Concrete", *Mechanics of Materials*, Vol. 24, No. 4, pp. 241-257.

Perzyna, P. (1966). “Fundamental problems in viscoplasticity”, *Advances in Applied Mechanics*, Vol. 9, pp. 243-377.

Schapery, R.A. (1984). “Correspondence principles and a generalized J-integral for large deformation and fracture analysis of viscoelastic media”, *Int. J. Fract.*, Vol. 25, pp.195-223.

Schapery, R.A. (1990). “A Theory of Mechanical Behavior of Elastic Media with Growing Damage and Other Changes in Structure”, *J. Mech. Phys. Solids*, 38, pp.215-253.

Schwartz, C.W., Gibson, N.H., Schapery, R.A., and Witczak, M.W., "Viscoplasticity Modeling of Asphalt Concrete Behavior," Recent Advances in Material Characterization and Modeling of Pavement Systems (Tutumluer, E., Masad, E., and Najjar, Y., ed.), *Geotechnical Special Publication 123*, ASCE, pp. 144-159.

Seibi, A. C., Sharma, M. G., Ali, G. A., and Kenis, W. J. (2001). “Constitutive relations for asphalt concrete under high rates of loading”, *Transportation Research Record*, Vol. 1767, pp. 111-119.

Tashman, L., Masad, E., Zbib, H., Little, D., and Kaloush, K. (2005). “microstructural viscoplastic continuum model for permanent deformation in asphalt pavements”, *Journal of Engineering Mechanics*, ASCE, Vol. 131(1), pp. 48-57.

Wang, L.B., Frost, J.D. and Shashidhar, N. (2001). Microstructure Study of Westrack Mixes from X-ray Tomography Images. TRR No.1767, pp85-94.

Wang, L.B. (2003). Stress Concentration Factor of Poroelastic Material by FEM Simulation and X-ray Tomography Imaging. ASCE Engineering Mechanics Conference, Seattle, WA.

Wang, L.B., Harold S. Paul, Thomas Harman and John D’Angelo (2004). Characterization of Aggregates and Asphalt Concrete using X-ray Tomography, AAPT, Vol. 73, pp. 467-500.

Wijk, G. (1978), “Some New Theoretical Aspects of Indirect Measurements of the Tensile Strength of Rocks”, *Int. J. Rock Mech. Min. Sci. & Geomech. Abstr.*, Vol. 15, pp.149-160.

Zhang, W. and Drescher, A. and Newcomb, D. E. (1997), “Viscoelastic Analysis of Diametral Compression of Asphalt Concrete”, *Journal of Engineering Mechanics*, Vol. 123, No. 6, pp.596-603.

Table 1 Stress concentration of the three WesTrack mixtures

Mixture	Phases[1]	Average	Maximum	S.C.F.[2]
Fine	2	0.0363	0.0658	1.81
	3	0.0333	0.0728	2.18
Fine Plus)	2	0.0337	0.0641	1.90
	3	0.0362	0.1985	5.48
3(Coarse)	2	0.0313	0.0676	2.16
	3	0.0354	0.2144	6.05
Theoretical solution		0.0364	0.0375	1.03

[1] 2 phases: binder+voids, aggregates
3 phases: aggregates, binder, voids
[2] Stress concentration factor.

Table 2 Stress statistic study for the fine-mix sample

Segment	before void removal			after void removal		
	Average	Maximum	S.C.F.	Average	Maximum	S.C.F.
1	0.03638	0.06577	1.81	0.03499	0.06840	1.95
2	0.03591	0.04486	1.25	0.03108	0.04284	1.38
3	0.03647	0.05088	1.40	0.03236	0.07280	2.25
4	0.03738	0.06138	1.64	0.03077	0.05027	1.63
5	0.03639	0.06064	1.67	0.02723	0.04643	1.71
6	0.03715	0.05797	1.56	0.04224	0.07277	1.72
7	0.03665	0.05287	1.44	0.03879	0.05836	1.50
8	0.03590	0.06026	1.68	0.03510	0.06213	1.77
9	0.03493	0.05057	1.45	0.02866	0.04429	1.55
10	0.03576	0.06429	1.80	0.03200	0.05744	1.79
STDEV	0.07%	0.68%	18.24%	0.46%	1.14%	24.61%

Table 3 Stress statistic study for the fine-plus mix sample

Segment	before void removal			after void removal		
	Average	Maximum	S.C.F.	Average	Maximum	S.C.F.
1	0.03519	0.05505	1.56	0.03931	0.07033	1.79
2	0.03331	0.05491	1.65	0.01387	0.03542	2.55
3	0.03452	0.05704	1.65	0.03694	0.08786	2.38
4	0.03328	0.06415	1.93	0.04403	0.16453	3.74
5	0.03161	0.05040	1.59	0.02370	0.12659	5.34
6	0.03287	0.05068	1.54	0.04236	0.10995	2.60
7	0.03365	0.05140	1.53	0.03826	0.19846	5.19
8	0.03327	0.05574	1.68	0.04221	0.10105	2.39
9	0.03532	0.05204	1.47	0.04277	0.12222	2.86
10	0.03403	0.05656	1.66	0.03864	0.10459	2.71
STDEV	0.11%	0.41%	12.51%	0.97%	4.58%	121.38%

Table 4 Stress statistic study for coarse-mix sample

Segment	before void removal			after void removal		
	Average	Maximum	S.C.F.	Average	Maximum	S.C.F.
1	0.03312	0.05041	1.52	0.04467	0.10635	2.38
2	0.03398	0.06763	1.99	0.03856	0.18578	4.82
3	0.03186	0.04622	1.45	0.02858	0.10865	3.80
4	0.03352	0.05181	1.55	0.03000	0.09078	3.03
5	0.03178	0.04507	1.42	0.02636	0.11865	4.50
6	0.03021	0.05118	1.69	0.03716	0.16080	4.33
7	0.02723	0.04594	1.69	0.04396	0.21444	4.88
8	0.03121	0.05546	1.78	0.03292	0.13823	4.20
9	0.03018	0.04060	1.35	0.03666	0.16088	4.39
10	0.02968	0.05724	1.93	0.03563	0.12001	3.37
STDEV	0.20%	0.77%	21.72%	0.61%	3.93%	81.57%

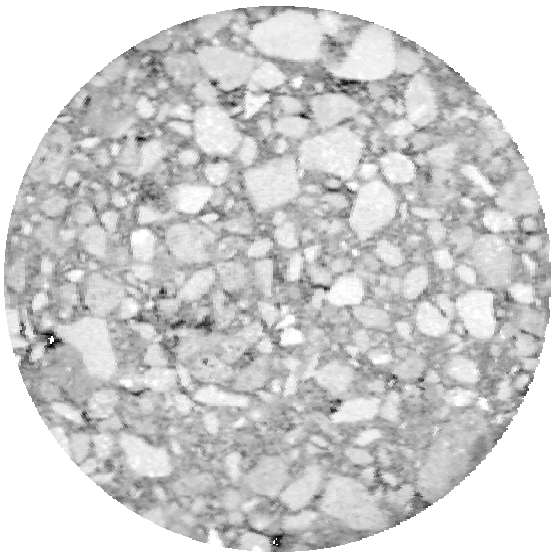

Figure 1 Gray image from x-ray scan

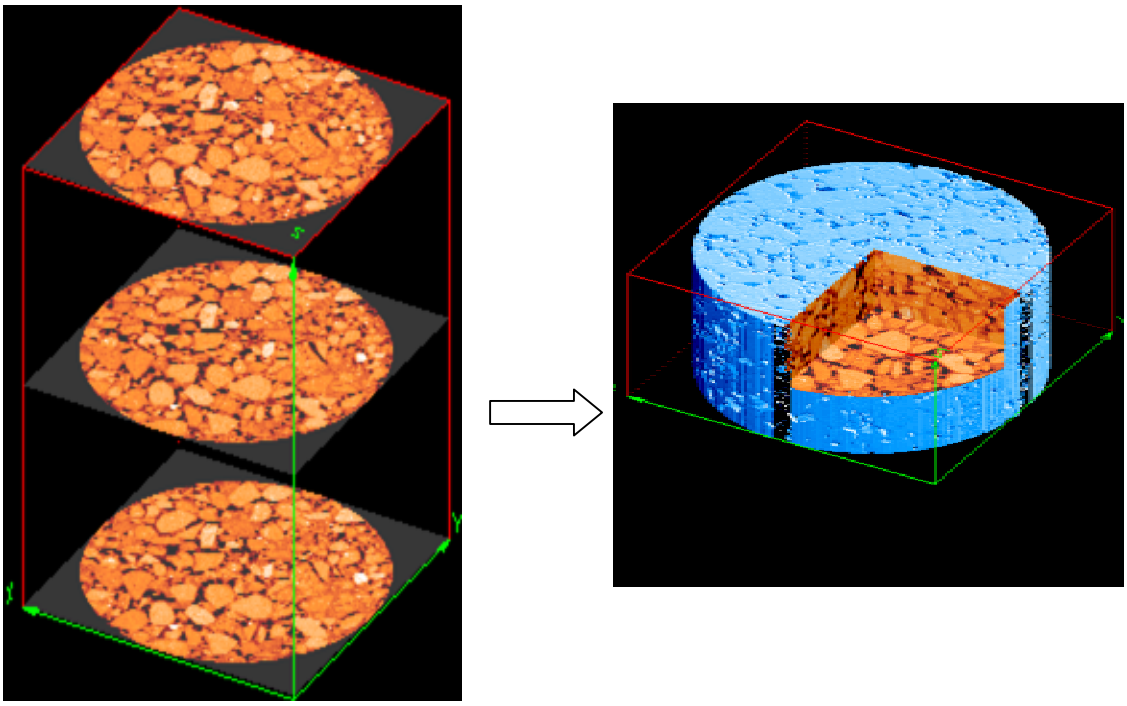

Figure 2 Reconstruction of three-dimensional microstructure

Stress notation used in following graphs:

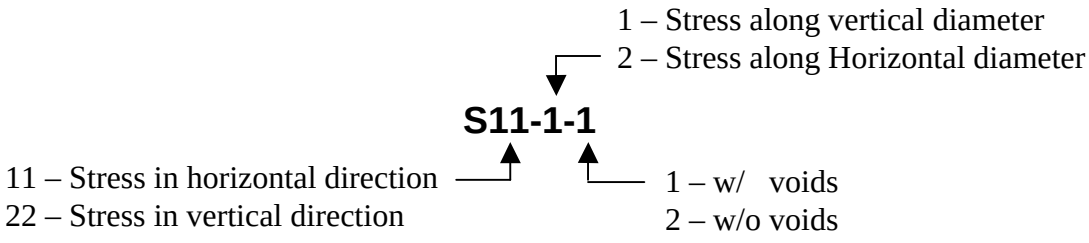

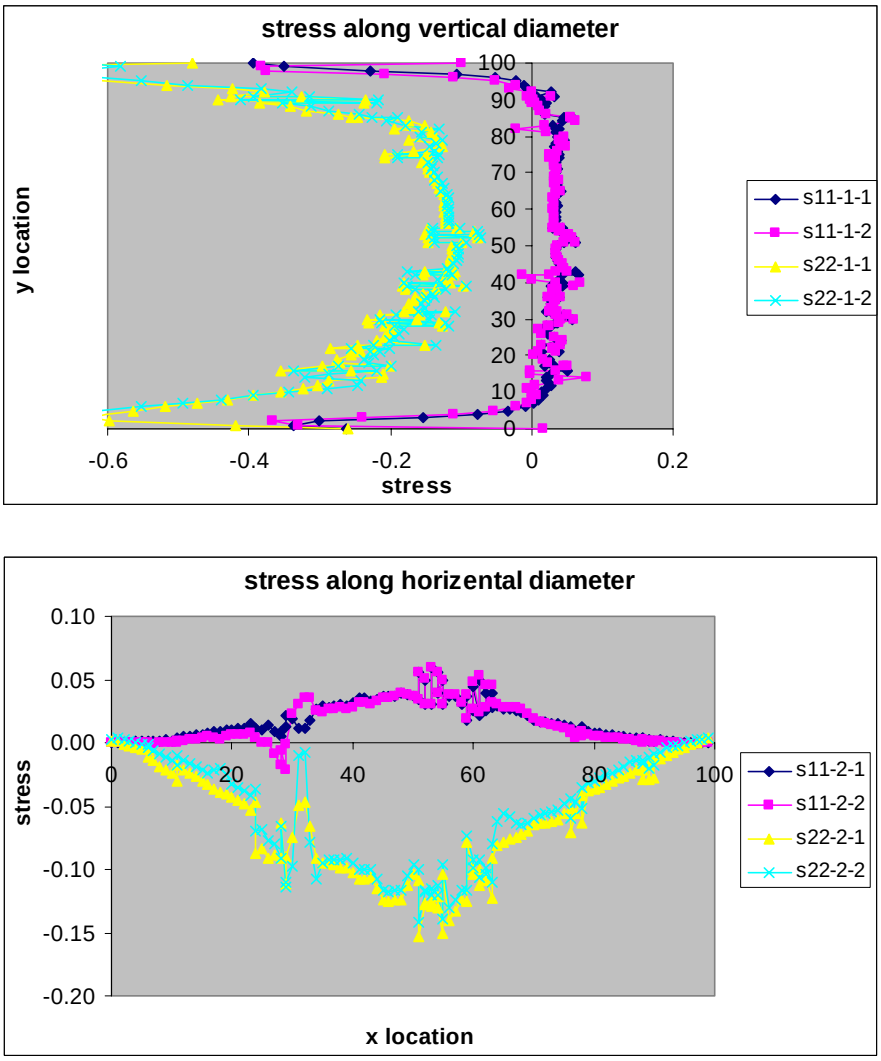

Figure 3 Stresses distribution for the fine-mix sample

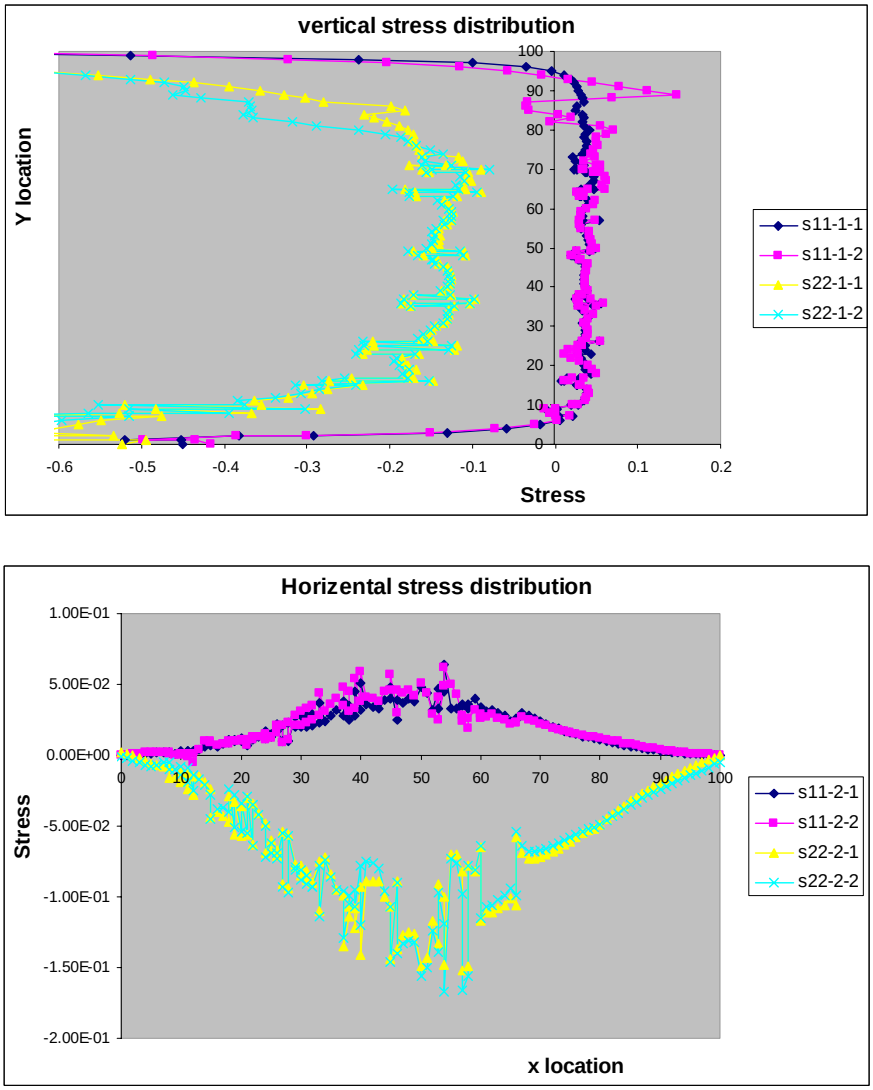

Figure 4 Stresses distribution for the fine-plus mix sample

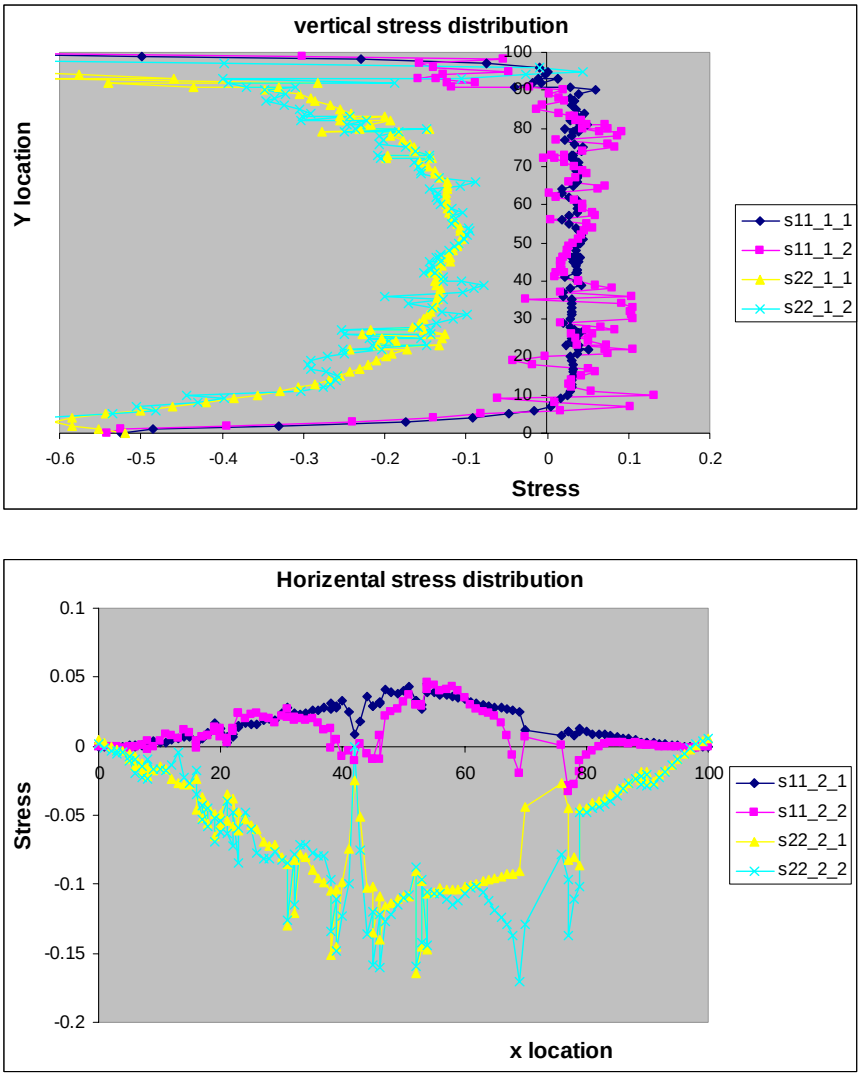

Figure 5 Stresses distribution for coarse-mix sample

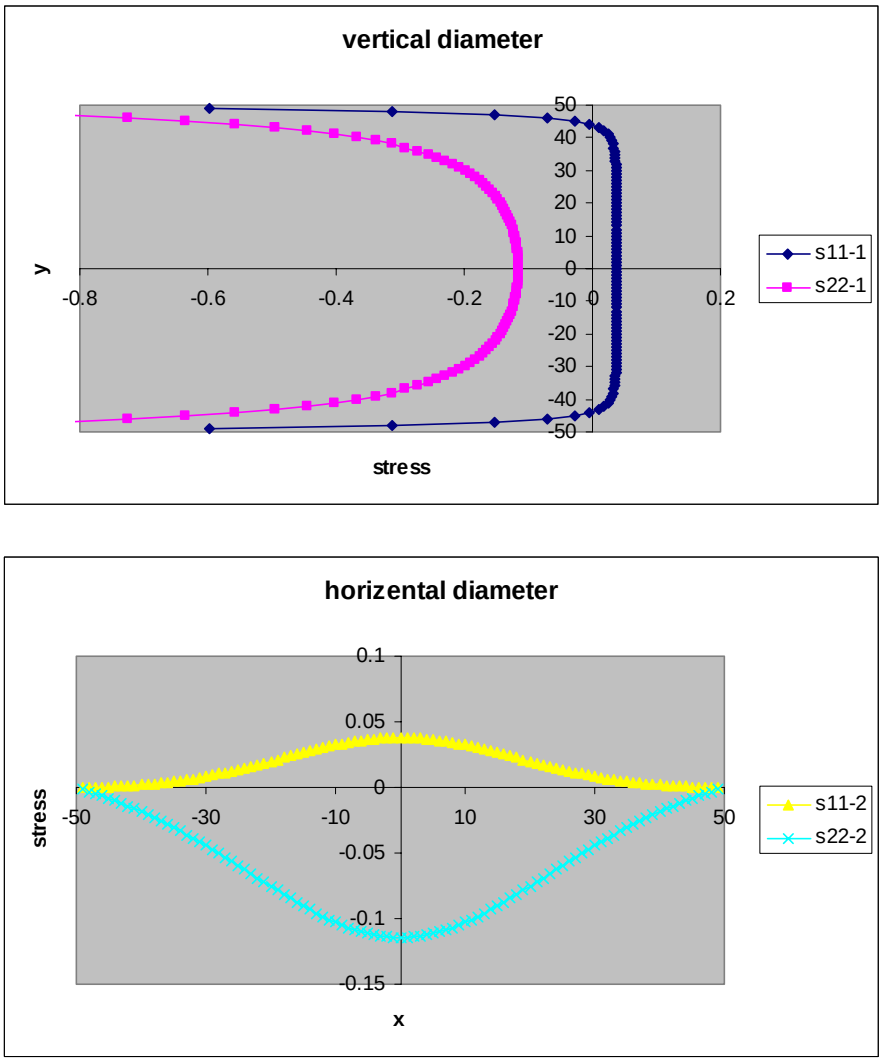

Figure 6 Stresses distribution along sample diameters (theoretical solution)

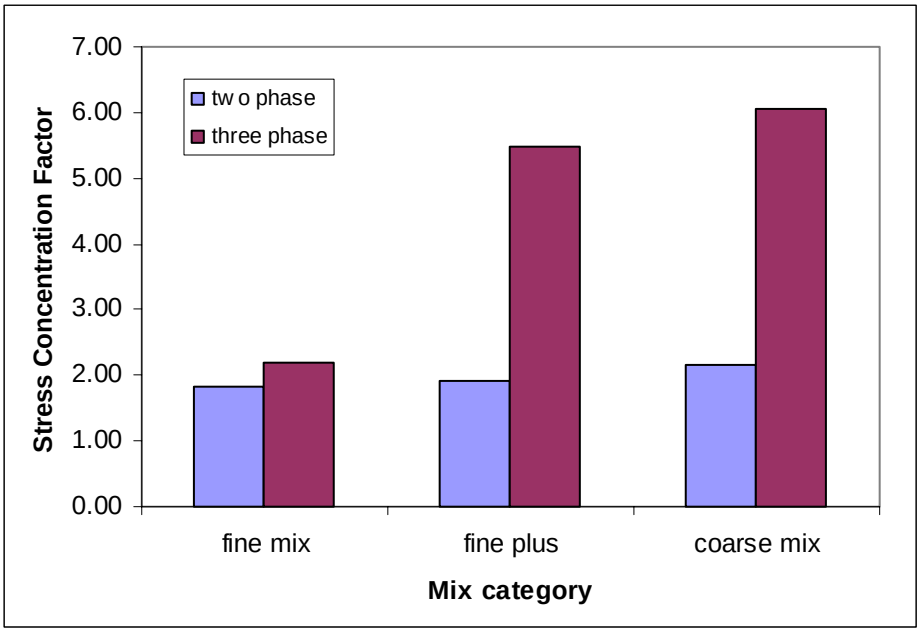

Figure 7 Stress concentration comparison

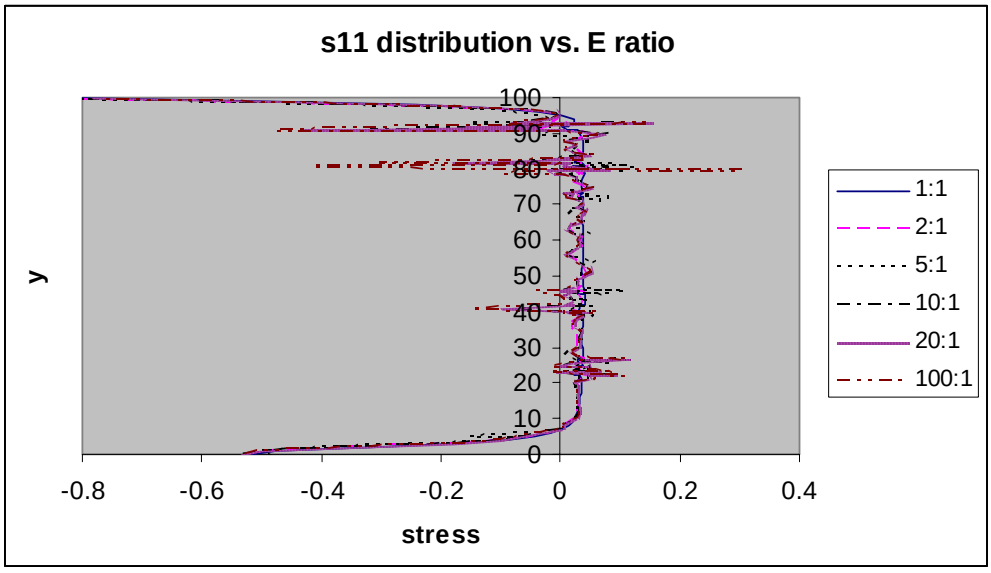

Note: s11 along vertical diameter with voids removed

Figure 8 Stress distribution for different E ratios